Heliyon 9 (2023) e23267

Contents lists available at ScienceDirect

Heliyon

journal homepage: www.cell.com/heliyon

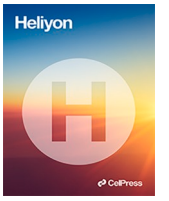

Comprehensive analysis of mitophagy-related subtypes of breast cancer and the association with immune related characteristics

Yaqing Zhou [a], Xing Wei [b], Weimiao Li [a], Shuqun Zhang [a], Yonglin Zhao [a,*]

[a] Department of Oncology, the Second Affiliated Hospital of Xi'an Jiaotong University, Xi'an, China
[b] Department of Gynaecology and Obstetrics, the Second Affiliated Hospital of Xi'an Jiaotong University, Xi'an, China

ARTICLE INFO

Keywords:
Breast cancer
Mitophagy
Subtypes
Tumor microenvironment
Precise treatment

ABSTRACT

Breast cancer (BRCA) is a common neoplasm characterized by high levels of molecular heterogeneity. Previous studies have noted the importance of mitophagy for the progression and prognosis of BRCA. However, little was found in the similarity and difference of mitophagy-related gene expression patterns of BRCA. This study intended to investigate the differences in functional activation, somatic mutation, and immune-related characteristics among different subtypes of BRCA associated with mitophagy. Based on bioinformatics analysis, we systematically examined the heterogeneity of breast cancer concerning mitophagy and observed two distinct subtypes with different tumor microenvironments and prognoses. BRCA samples from TCGA database were divided into two subtypes based on the expression of 29 mitophagy-related genes by ConsensusClusterPlus algorithm. Two mitophagy-related subtypes with marked prognostic discrepancies were significantly correlated with race, intrinsic subtype grouped based on PAM50 subtype purity and BRCA Pathology. The results of GSVA and immune microenvironment analysis showed significant differences in cancer-related and immune-related features between the two subtypes. METABRIC datasets were extracted to validate the immune characteristics scoring and the expression of immune checkpoints between different subtypes based on the medium value of TCGA-Mitophagy score. It is noteworthy that the present study is the first to demonstrate a new classification based on the mitophagy of breast cancer, which comes up with a new perspective for the assessment and prognoses of BRCA.

1. Introduction

Breast cancer (BRCA) has become the most commonly diagnosed tumor in the world, with the number of new cases around the world up to 2.26 million according to the latest global statistical data in 2020. Meanwhile, BRCA has become the leading cause of cancer mortality in women worldwide [1]. BRCA has high molecular-level heterogeneity, and tumor heterogeneity is closely associated with the tolerance of therapy [2]. Pathological typing combined with molecular markers is the usual diagnostic method for BRCA. In clinical practice, BRCA is categorized as luminal A-like, luminal B-like, basal-like and HER2-enriched type according to the status of ER, PR and HER2 [3,4]. Compared with other malignant tumors, the diagnosis and treatment for BRCA are more established and standardized, but the status of patients with advanced breast cancer is still not optimistic. The improvement of individualized treatment for BRCA is partly based on the progression of biological markers and mechanisms, and new subtypes or markers thus need

* Corresponding author. The Second Affiliated Hospital of Xi'an Jiaotong University, No.157 XiwuRoad, Xi'an, 710004, China.
E-mail address: zyl2018@xjtu.edu.cn (Y. Zhao).

https://doi.org/10.1016/j.heliyon.2023.e23267
Received 26 January 2023; Received in revised form 26 November 2023; Accepted 29 November 2023
Available online 3 December 2023

to be further explored [5,6].

Autophagy is a self-degradation of cells, most of which are non-selective for cytosolic cargo [7], but some are targeted to engulf and degrade specific cargoes, such as mitophagy. Mitophagy is a particular autophagy form, in which mitochondria are selectively degraded by autophagolysosome [8]. Generally, mitophagy plays an essential role in removing dysfunctional mitochondria to sustain normal function and restrict the generation of ROS. Moreover, mitophagy can also reduce excess mitochondria, improve the adaptation to hypoxia and nutrient deprivation, and further limit the production of excessive ROS [9]. Further research has revealed that the role of mitophagy in tumor growth, metastasis and therapy resistance is very important, but the function of mitophagy is complex, and its pro- or anti-tumor effect may be based on the stage, type, metabolism or microenvironment of the tumor [10]. Although we had some realization of the relationship between mitophagy and cancer, the specific mechanisms of every tumor are unclear due to the complexity and variety of mitophagy, such as in BRCA. Mitophagy may be a valid and more targeted therapy for BRCA. Depending on the differentially expressed genes (DEGs) of mitophagy-related tumor classification, 13-gene signature was built as a novel biomarker for the prognosis of BRCA and provided a systemic analysis of therapy response [11].

Although prognostic models can provide more direct predictive information and clinical applications for tumors, the challenges of model complexity and large sample requirements were not ignored. In the present study, we aimed to further explore the functional activity, genetic and immune characteristics of different mitophagy-related subtypes. To assess the similarity and difference between BRCA samples in terms of mitophagy-related gene expression and immune-related characteristics, we used consensus clustering algorithm to classify BRCA samples. We divided 1076 BRCA samples into two clusters based on the expression of 29 mitophagy-related genes. Then, we analyzed progression, clinical and biological characteristics, and immune features of two subtypes. Finally, we assessed the therapeutic sensitivity of the two mitophagy-related subtypes. These results further proved the cluster was reasonable and practicable.

2. Materials and methods

2.1. Data source

In the present study, we downloaded the transcriptomic data, copy number variation (CNV) data, and clinical information of 1076 BRCA samples from The Cancer Genome Atlas (TCGA, https://portal.gdc.cancer.gov/). The somatic mutation data of 988 cases of these BRCA samples were also downloaded for mutation analysis. The 29 mitophagy-related genes (MRGs) were extracted from the mitophagy (R-HSA-5205647), PINK1-PRKN mediated mitophagy (R-HSA-5205685) and receptor-mediated mitophagy (R-HSA-8934903) pathways from the Reactome database after de-duplication according to the previous study [12]. METABRIC dataset containing 1980 BRCA samples was downloaded from cBioPortal as an external validation dataset.

2.2. Identification of mitophagy-related molecular subtypes of BRCA

Based on the expression profiles of 28 MRGs expressed in TCGA datasets, the 1076 BRCA samples were classified by consensus clustering algorithm using the 'ConsensusClusterPlus' package (version 1.54.0) K-means clustering algorithm was employed to stratify the data into a given number of robust clusters setting 'maxK' as 6 [13]. The cumulative distribution function (CDF) curve and CDF delta area curve were plotted to determine the optimal number of mitophagy-related subtypes. Consensus matrix heatmap was generated for representation of cluster membership. Next, the principal component analysis (PCA) and uniform manifold approximation and projection (UMAP) analyses were implemented to visualize the distribution of different subtypes of samples. Besides, the gene expression of MRGs and survival differences between different subtypes were examined through pheatmap (version 1.0.12) and survival (version 3.2–11), respectively.

2.3. Correlation analysis of clinical characteristics

The R package ComplexHeatmap (version 2.12.0) was utilized to plot the clinical trait heatmap [14]. Using the R package ggstatsplot (version 0.9.1), histograms of the proportion of the number of patients with clinical traits were plotted between different mitophagy-related molecular subtypes. The clinical factors that differed in the number of patients between different mitophagy-related molecular subtypes were determined by chi-square tests.

2.4. Somatic mutation and copy number variation (CNV) analysis

Single-nucleotide polymorphisms (SNPs) mutation analysis was processed with the 'maftools' R package (version 2.12.0) [15]. CNV analysis was conducted in 'GISTIC2.0' (version 2.0.22) [16]. The mutation lanscape and proportions of mutation types between the mitophagy gene subtypes was compared.

2.5. Gene set variation analysis (GSVA)

The GSVA algorithm in the R 'GSVA' package (version 1.42.0) was applied to calculate the pathway and immune signature scores for each tumor sample based on the 'Hallmark gene sets' downloaded from the MsigDB database (https://www.gsea-msigdb.org/), the 13 oncogenic hallmarks, epithelial-to-mesenchymal transition (EMT), and cancer stem cell (CSC) signatures provided by Sanchez-Vega

et al. [17], and the 3 immune-related functional signatures provided by Bindea and Thorsson, including Immune suppression, Cytolytic Activity, and Antigen Processing Machinery [18,19]. The heatmap and box plot were graphed by R 'pheatmap' package (version 1.0.12) and 'ggpubr' package (version 0.4.0) respectively. The differences between different subtypes were compared using the

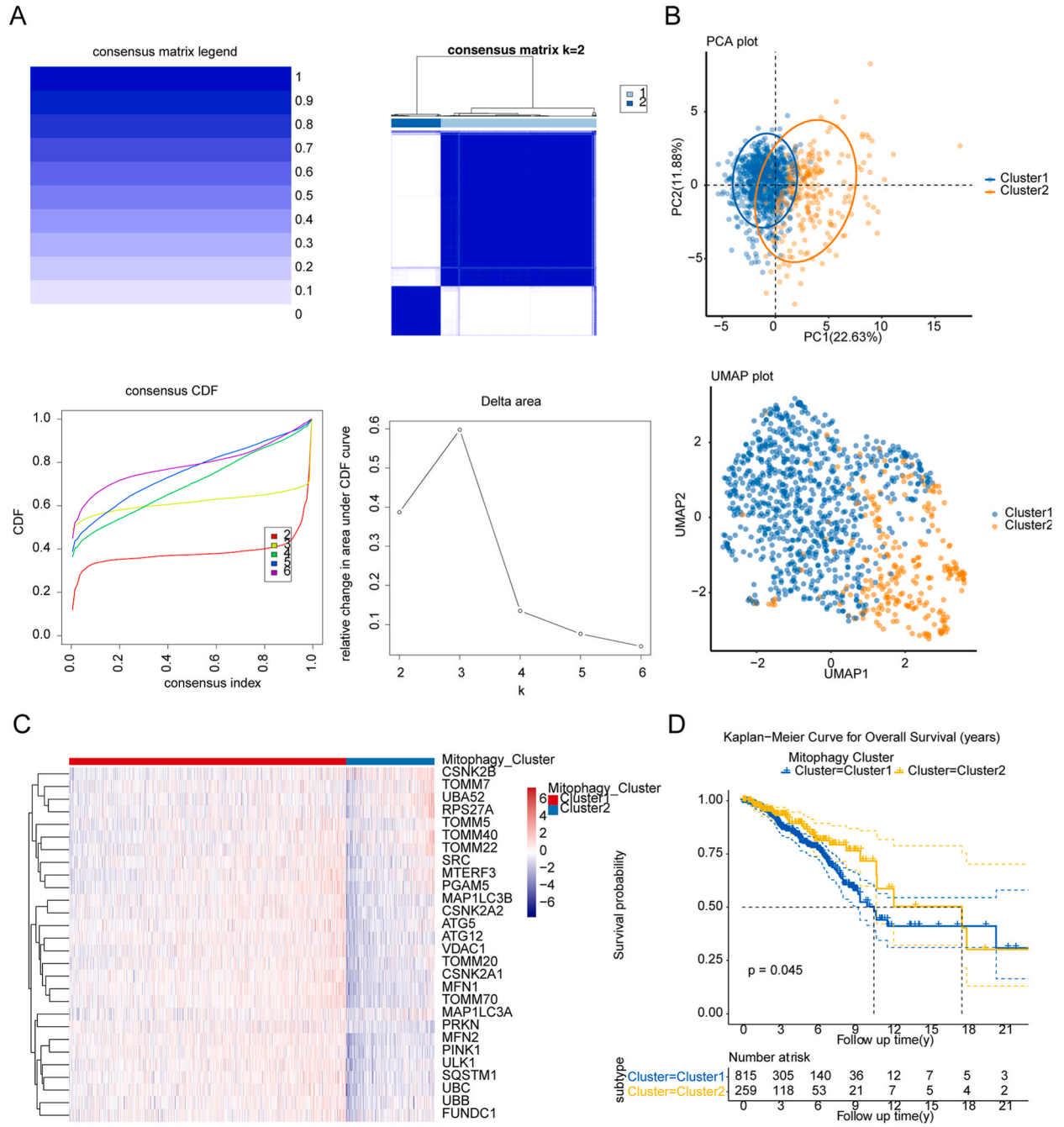

Fig. 1. The mitophagy-related molecular subtypes of breast cancer. (**A**) Consensus clustering of 1076 samples in TCGA-BRCA based on mitophagy-related genes. The cumulative distribution function (CDF) diagram revealed that the CDF curve remains relatively flat at K = 2, the abscissa is the consistency index, indicating the difficulty of clustering. The relative change of the area under the CDF curve between K and K-1 indicates a more pronounced slope change after K values of 2 and 3. Therefore, K = 2 were chosen as the optimal number of clusters and consistency matrix was exhibited. The numbers on the right is the value of k, the rows and columns of the matrix represent samples, the values of the matrix are represented from 0 to 1 in white to dark blue. (**B**) Principal component analysis (PCA) and uniform manifold approximation and projection (UMAP) diagram of the two clusters in TCGA-BRCA. Cluster1: blue; Cluster2: yellow. (**C**) The expression heatmap of 28 mitophagy-related genes in two clusters. 28 genes were used as sample annotations, red represents cluster1 and blue represents cluster2. (**D**) The survival curves of two clusters.

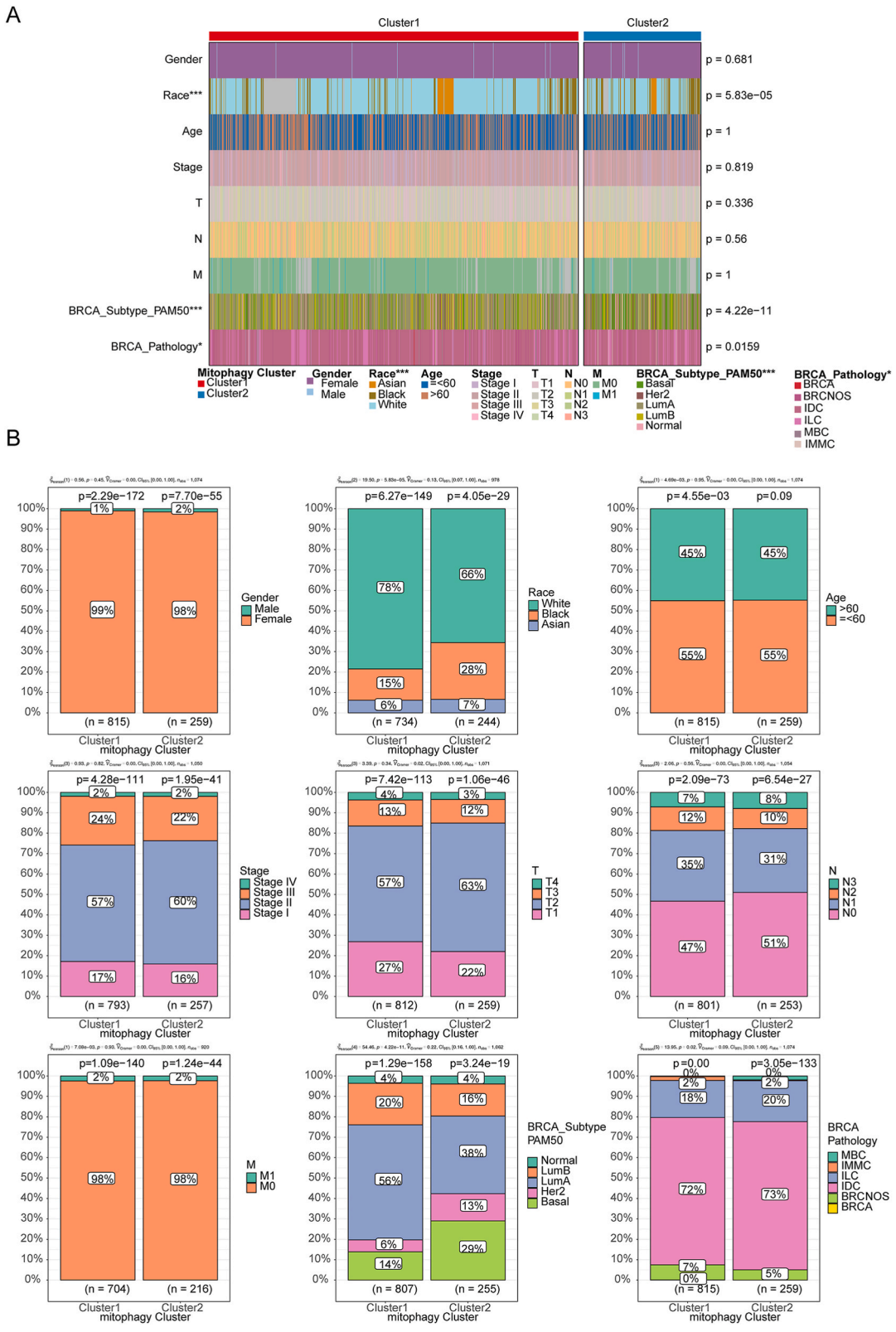

Fig. 2. The clinical characteristics of two subtypes. (**A**) The heatmap of the correlation between clinical factors and autophagy-related subtypes. (**B**) The proportion of samples in two clusters for each clinical data were compared using chi-square tests.

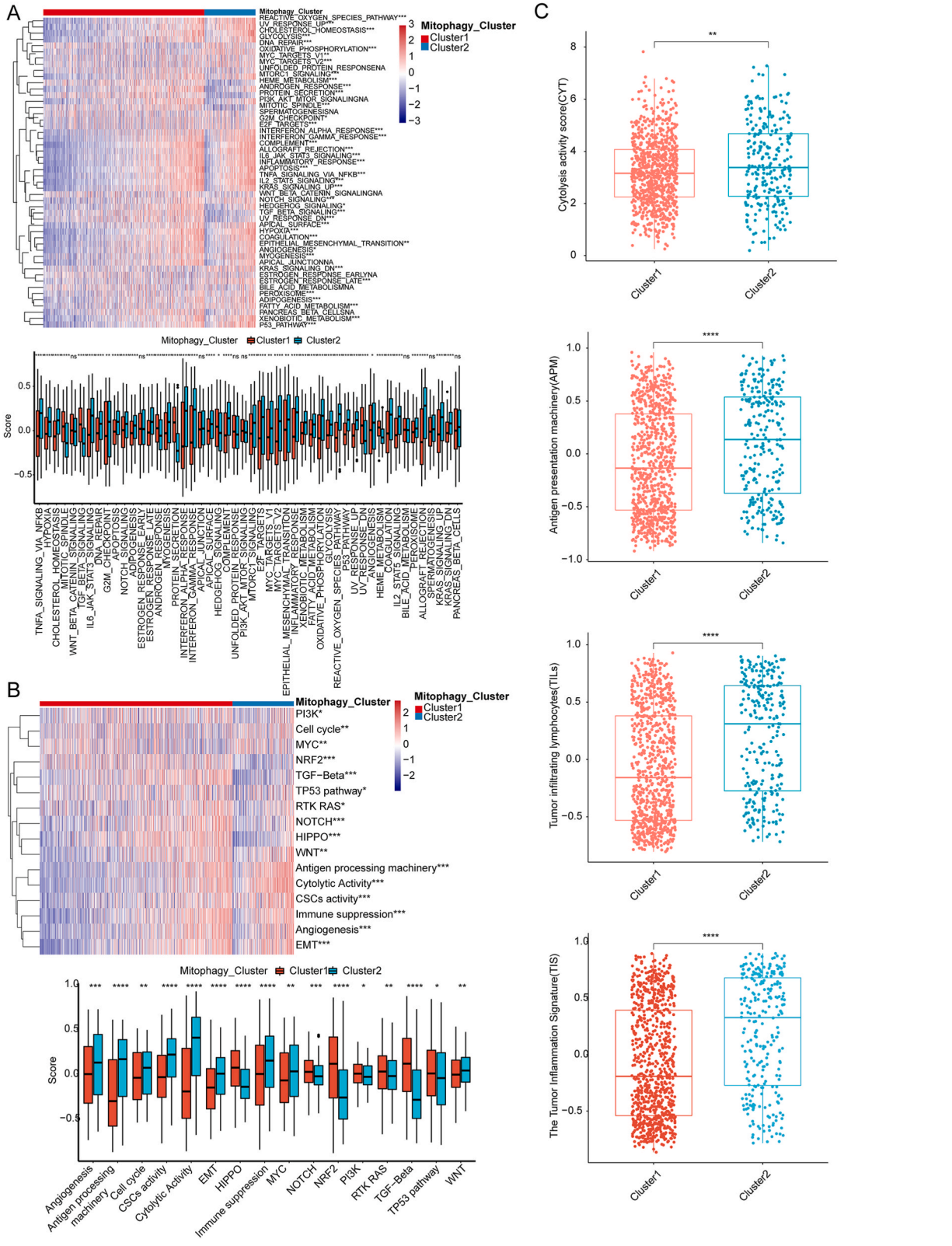

(caption on next page)

Fig. 3. Gene set variation analysis (GSVA) of mitophagy-related subtypes. (**A**) Heatmap and boxplot for differences in gene pathway enrichment scoring of Hallmark gene sets between two clusters. (**B**) Heatmap and boxplot for differences in enrichment scoring of 13 oncogenic-related and three immune-related functional pathways between two clusters. The statistical differences between the two clusters were tested by the Wilcoxon test. (*P < 0.05; **P < 0.01; ***P < 0.001; ****p < 0.0001; ns, non-significant). (**C**) The immune characteristics of two subtypes, including Cytolytic (CYT) activity score, Antigen Presentation Machinery (APM) score, Tumor infiltrating lymphocytes (TILs) levels and Tumor Inflammation Signature (TIS).

Wilcoxon test. Further, Cytolytic (CYT) activity score was calculated based on the geometric mean of TPM expression of GZMA and PRF1, Antigen Presentation Machinery (APM) score, Tumor infiltrating lymphocytes (TILs) levels and Tumor Inflammation Signature (TIS) were calculated using GSVA method to compare the differences in four immune markers infiltrating profiles.

2.6. Tumor microenvironment (TME) analysis

The immune score, stromal score, ESTIMATE score, and tumor purity for each BRCA sample were computed by the 'ESTIMATE' R package (version 1.0.13) [20]. Through the CIBERSORT algorithm [21], fraction of immune infiltrating cells were calculated for each BRCA sample. The differences between different subtypes were compared using the Wilcoxon test.

2.7. Therapy analysis

The TIDE website was utilized to infer and assess the sensitivity of each subtype to immune checkpoint blockade (ICB) therapy [22]. Via the 'pRRophetic' package (version 0.5) [23], we computed IC_{50} values for 138 chemotherapy drugs for two subtypes of patients to speculate on their sensitivity to chemotherapy. The differences between different subtypes were compared using the Wilcoxon test.

2.8. Verify of the immune related scores via the METABRIC cohort

METABRIC datasets were extracted to validate the immune characteristics and the expression of immune checkpoints between different subtypes. Firstly, using PCA reduction techniques to reduce the dimensionality of the METABRIC datasets and improve the classification effect. Next, we defined the sum of the first principal component variable in the TCGA-PCA (PC1) and the second principal component variable (PC2) as Mitophagy score. Based on the median value of the TCGA-mitophagy score, the samples in the METABRIC dataset were grouped based on the sum of PC1 and PC2 (Mitophagy score) of each sample calculated in METABRIC-PCA. Wilcoxon test was utilized to explore the levels of four immune markers and three immune checkpoints.

2.9. Statistical analysis

The R programming language was used to conduct all analyses, and the data from different groups were compared by the Wilcoxon test and chi-square tests was used for the differences in clinical characteristics. If not specified above, a p-value less than 0.05 was considered statistically significant.

3. Results

3.1. Recognition of mitophagy-related molecular subtypes of BRCA

Based on the expression of 29 mitophagy-related genes extracted from the Reactome database, consensus clustering was conducted to determine the optimal number of mitophagy-related subtypes. The cumulative distribution function (CDF) diagram revealed that the CDF curve remains relatively flat at K = 2, suggesting a high level of clustering consistency. And meanwhile, the area under CDF curve diagram indicates a more pronounced slope change after K values of 2 and 3. Therefore, K = 2 were chosen as the optimal number of clusters, and 1076 BRCA samples were clustered into two clusters by consistent clustering, with cluster1 containing 816 samples and cluster2 containing 260 samples, respectively (Fig. 1A). PCA and UAMP dimensionality reduction analysis demonstrated that two clusters were located at different positions and could be clearly distinguished, indicating a credible result for clustering (Fig. 1B). By observing the gene expression and survival differences between the two groups, the heatmap revealed that mitophagy-related genes were highly expressed in cluster1 (Fig. 1C), and survival analysis demonstrated a significant survival discrepancy between the two subtypes as well (Log-rank test, $P = 0.045$), with worse survival for cluster1 (Fig. 1D).

3.2. Clinical features and biological functional characteristics of mitophagy-related subtypes

To better illuminate the distinctions between subtypes, we examined clinical data of TCGA and GSVA enrichment analysis was performed. Using the chi-squared test, it was found that there were a significant differences in the proportions of BRCA cohorts with different race ($P < 0.001$) between cluster1 and cluster2, as well as PAM50 molecular subgroups ($P < 0.001$), and BRCA Pathology subgroups ($P < 0.016$) (Fig. 2A and B and Table S1). Comparatively speaking, most white people tended to be in cluster1 (70.7 %). The percentage of luminal A type was highest in cluster1 (55.8 %). The main pathology of clusters was IDC, but less MBC in cluster2.

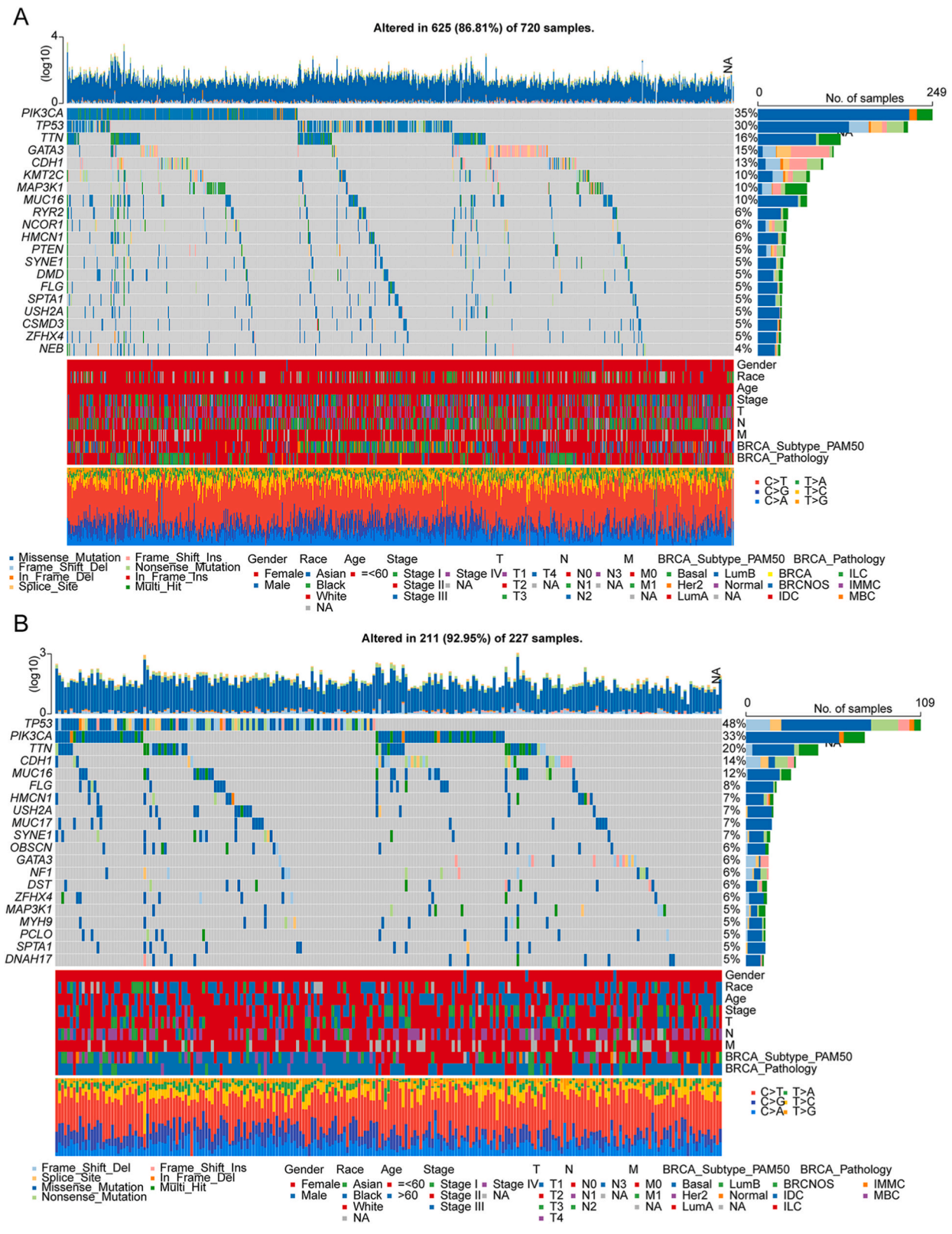

Fig. 4. Waterfall plot for the top 20 most frequently altered genes in different subtypes. (**A**) cluster1, (**B**) cluster2. Each column represents a sample with the stacked barplot on the bottom displaying the clinical data and the fraction of conversions for each sample. The barplot and the percentage numbers on the right display the proportion and mutation frequency of each gene in all samples, respectively.

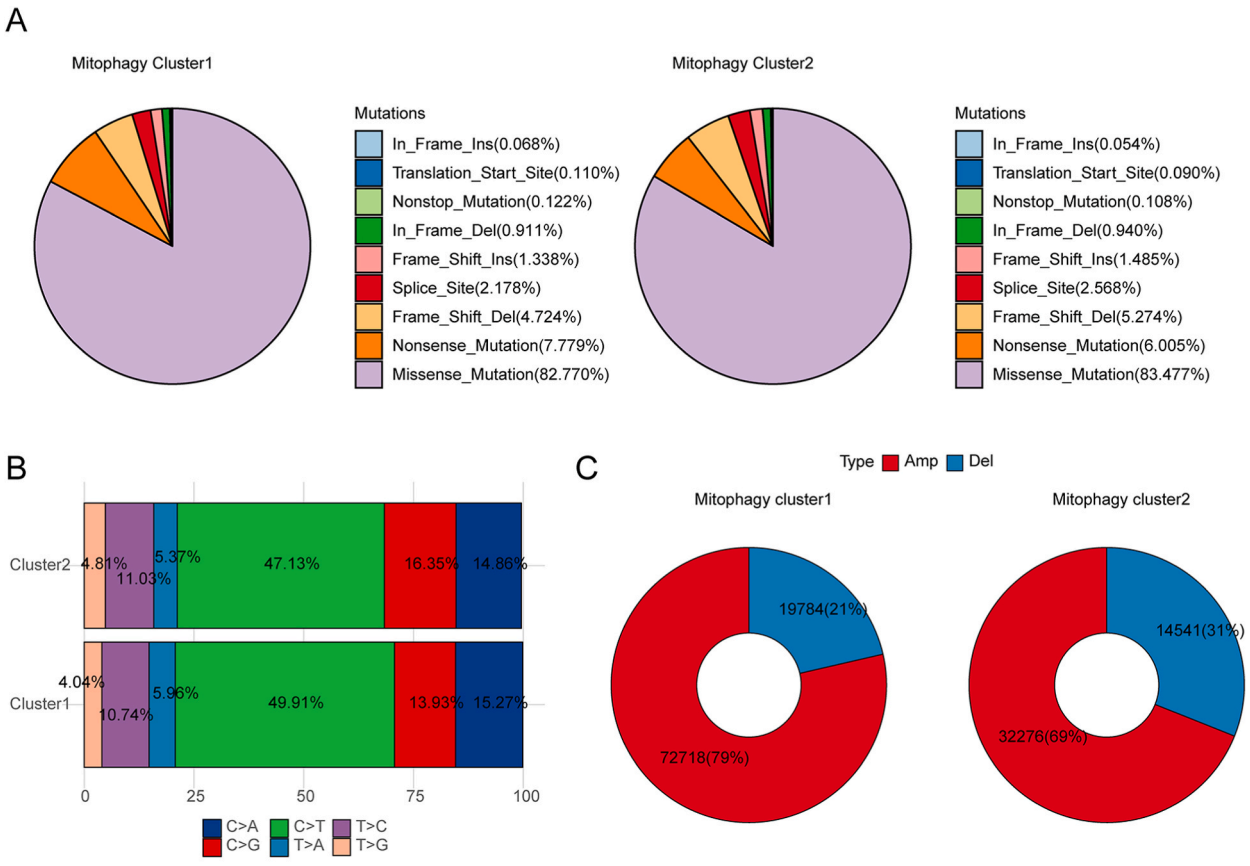

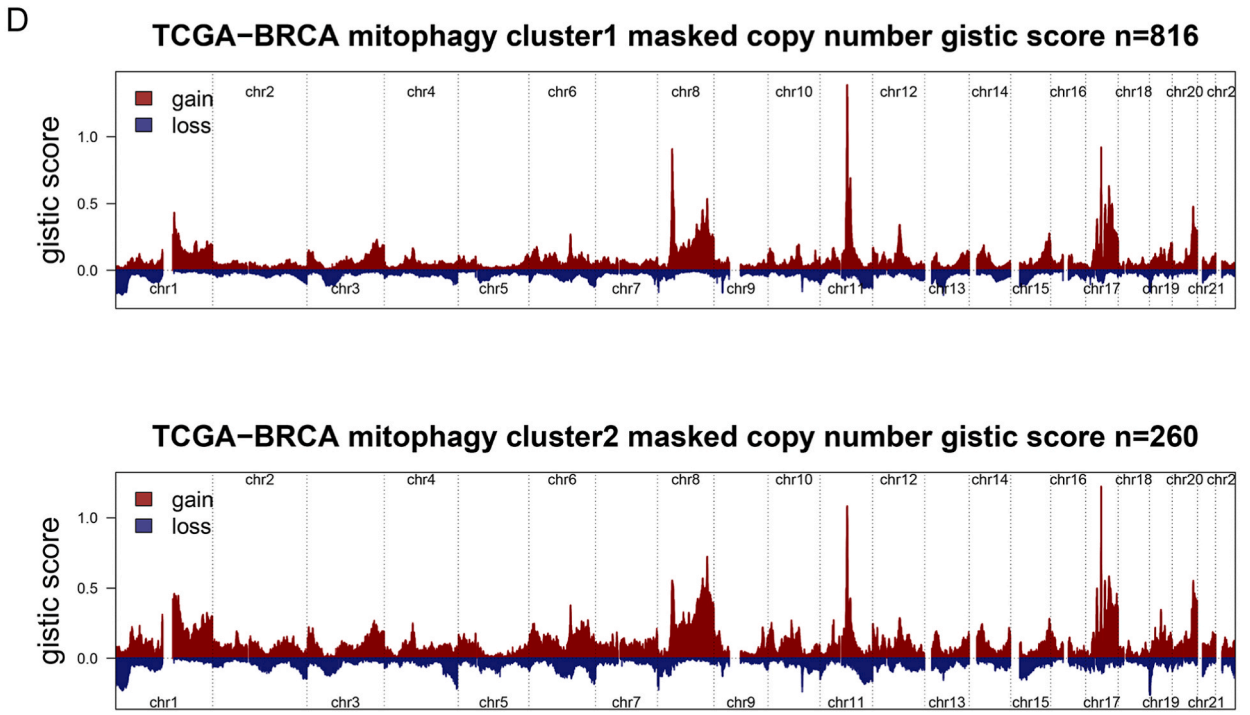

(caption on next page)

Fig. 5. The landscape of genetic alterations of two subtypes in TCGA-BRCA dataset. (**A**) The proportion of different mutation types in two mitophagy-related subtypes. (**B**) Comparing of the proportion of point mutation type between two mitophagy-related subtypes. (**C**) The proportion of amplifications and deletions between two mitophagy-related subtypes. (**D**) The amplification or deletion of regions on chromosomes of mitophagy-related subtypes.

For the gene pathway enrichment scoring of Hallmark gene sets between two clusters, 42 distinct Hallmark pathways were discovered using GSVA enrichment analysis, and as compared to cluster2, cluster1 was enriched in mitotic spindle ($P < 0.001$), TGF-signaling ($P < 0.001$), androgen response ($P < 0.001$) (Fig. 3A). Further elucidating the distinction in malignant pathways and immune pathways of subtypes, oncogenic hallmark data and immune-related functional pathways were analyzed, 13 oncogenic pathways and 3 immune-related functional pathways were all significantly different between two subtypes (Fig. 3B). Among them 'PI3K' ($P < 0.05$), 'NRF2' ($P < 0.001$), 'TGF-Beta' ($P < 0.001$), 'TP53 pathway' ($P < 0.05$), 'RTK RAS' ($P < 0.05$), 'NOTCH' ($P < 0.001$), and 'HIPPO' ($P < 0.001$) were enriched in cluster1, 'cell cycle' ($P < 0.01$), 'MYC ($P < 0.01$)', 'WNT' ($P < 0.01$), 'CSCs activity' ($P < 0.001$), 'angiogenesis' ($P < 0.001$), 'EMT' and all of 3 immune-related functional signatures ('antigen processing machinery', 'cytolytic activity', 'immune suppression') ($P < 0.001$) were enriched in cluster2. Considering the enrichement of the immune-related functions in cluster2, the infiltration scoring of four immune markers, including the CYT ($P < 0.01$), APM ($P < 0.0001$), TILs ($P < 0.0001$) and TIS ($P < 0.0001$) were analyzed for the immune characteristics of two clusters, cluster2 had noticeably higher grades (Fig. 3C), which implied cluster2 were more likely to have a higher anti-tumor immune activity.

3.3. Genomic background analysis of mitophagy-related subtypes

To further investigate the mutational discrepancy between the two mitophagy-related subtypes, we further proceeded with somatic mutation analysis and CNV analysis. The overall somatic mutation landscape of BRCA samples was shown in Fig. S1, and PIK3CA, TP53 and TTN were genes with the highest mutation frequency. As the waterfall plot of the top 20 mutated genes for two subtypes showed, the highest mutated gene in cluster1 was PIK3CA (35 %), and the highest mutated gene in cluster2 was TP53 (48 %) (Fig. 4A and B). Further, the proportion of variant classification for the two clusters was displayed as a pie chart in Fig. 5A, where missense mutation was the top variant classifications. On the other hand, given that the most predominant variant type of mutation was the SNP (Fig. S1), the type and proportion of SNV in two subtypes were analyzed, shere the top three SNV types with the highest incidence for cluster1 were C > T, C > A, and C > G, as for cluster2, the types were C > T, C > G and C > A (Fig. 5B). In addition, the proportions of significantly amplified or deleted genomic regions of CNV of two clusters was visualized using GISTIC 2.0, Compared with cluster2, cluster1 had a higher proportion of amplifications and a lower proportion of deletions (Fig. 5C). Besides, the distribution and scores of CNVs on chromosomes for the two clusters were shown in Fig. 5D.

3.4. Analysis of immune characteristics and immune microenvironment of mitophagy-related subtypes

Moreover, ESTIMATE was used to assess the proportion of immune cell and stromal cell, and tumor purity between clusters using Wilcoxon test. As shown in Fig. 6A, cluster2 had a significantly higher ESTIMATE score ($P < 0.001$) and Immune score ($P < 0.0001$) than cluster1 and a significantly lower tumor purity ($P < 0.001$) and Stromal score ($P < 0.038$) than cluster1.

Utilizing the CIBERSORT method and the LM22 gene signature, we calculated and compared the level of 22 immune cell infiltration in the two subtypes using the Wilcoxon test (where the content of naive CD4 T cells is 0) (Fig. 6B). As shown in the violin plot (Fig. 6C), the fraction of resting CD4 memory T cells, resting NK cells, M2 Macrophages, activated Dendritic cells, and resting Mast cells were elevated in cluster1, while the fraction of Plasma cells, CD8 T cells, activated CD4 memory T cells, follicular helper T cells, regulatory T cells (Tregs), gamma delta T cells, and activated NK cells were superior in cluster2 ($P < 0.05$).

3.5. The therapy analysis between the two mitophagy-related subtypes

Considering the importance of immune checkpoint inhibitors represented by PD-1/PD-L1 antibodies and immunotherapy in anti-tumor therapy, we examined the sensitivity of mitophagy-related subtypes to immunotherapy and chemotherapy. The expression of PD-1, PD-L1 and CTLA-4 between two subtypes were compared and the difference was demonstrated in Fig. 7A, the expressions of PD-1 ($P < 0.001$) and CTLA-4 ($P < 0.01$) were higher in cluster2 compared with cluster1, while the expression of PD-L1 ($P < 0.001$) was higher in cluster1 (Fig. 7A). TIDE can assess the possibility of tumor immune escape, where the TIDE value of cluster2 was higher (Fig. 7B). While, there few difference in response to immunotherapy in two clusters (Fig. 7C).

Moreover, by utilizing the GDSC database, we predicted the sensitivity of 138 drugs for two subtypes. A total of 118 drugs differed in sensitivity between the two subtypes, with cluster1 being more sensitive to 53 drugs and cluster2 being more sensitive to 59 drugs. The top 9 drugs with the highest sensitivity differences (sorted by p-value) were shown in Fig. 7D.

3.6. Validation in immune characteristics in METABRIC dataset based on TCGA-mitophagy score

Finally, via the PCA results of TCGA datasets in Figrue 1B, the sum of the PC1 and the PC2 in TCGA-PCA is defined as the Mitophagy score of the sample. Fig. S2A shows that the Mitophagy score significantly differed in the two autophagy-related clusters of the TCGA dataset ($P < 0.0001$). Then, according to the median value of TCGA mitophagy score, we grouped the samples based on the sum of PC1

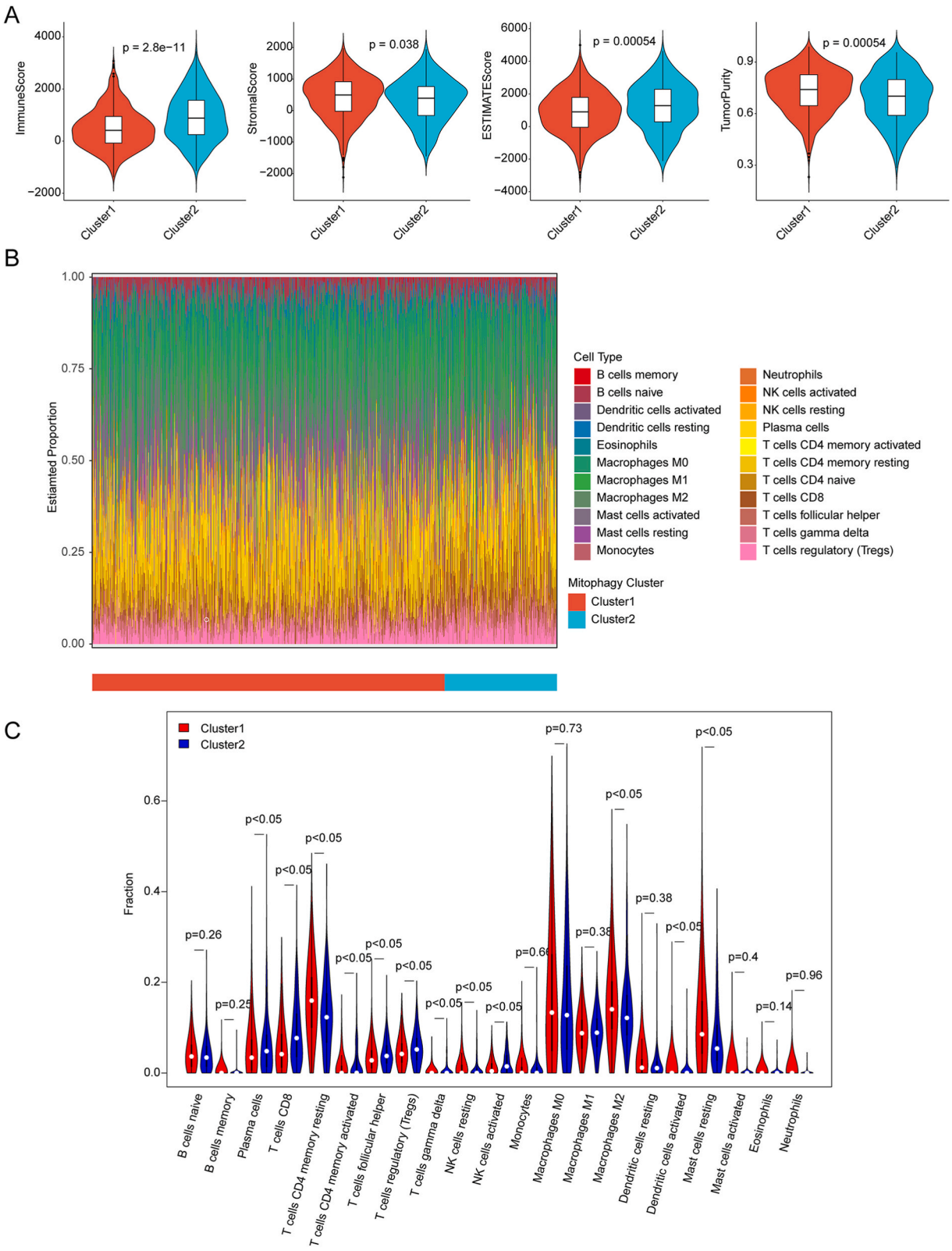

(caption on next page)

Fig. 6. The immune correlation analysis of two mitophagy-related subtypes. (**A**) The immune related scores of two subtypes, including stromal-score, immunescore, ESTIMATEscore and tumorpurity. (**B**) The proportion of 22 immune cells for each sample in TCGA-BRCA was assessed by CIBERSORT. (**C**) Violin plot for the fraction of 22 immune cells between two subtypes. The statistical differences between the two clusters were tested by the Wilcoxon test, statistical significance was set at $P < 0.05$.

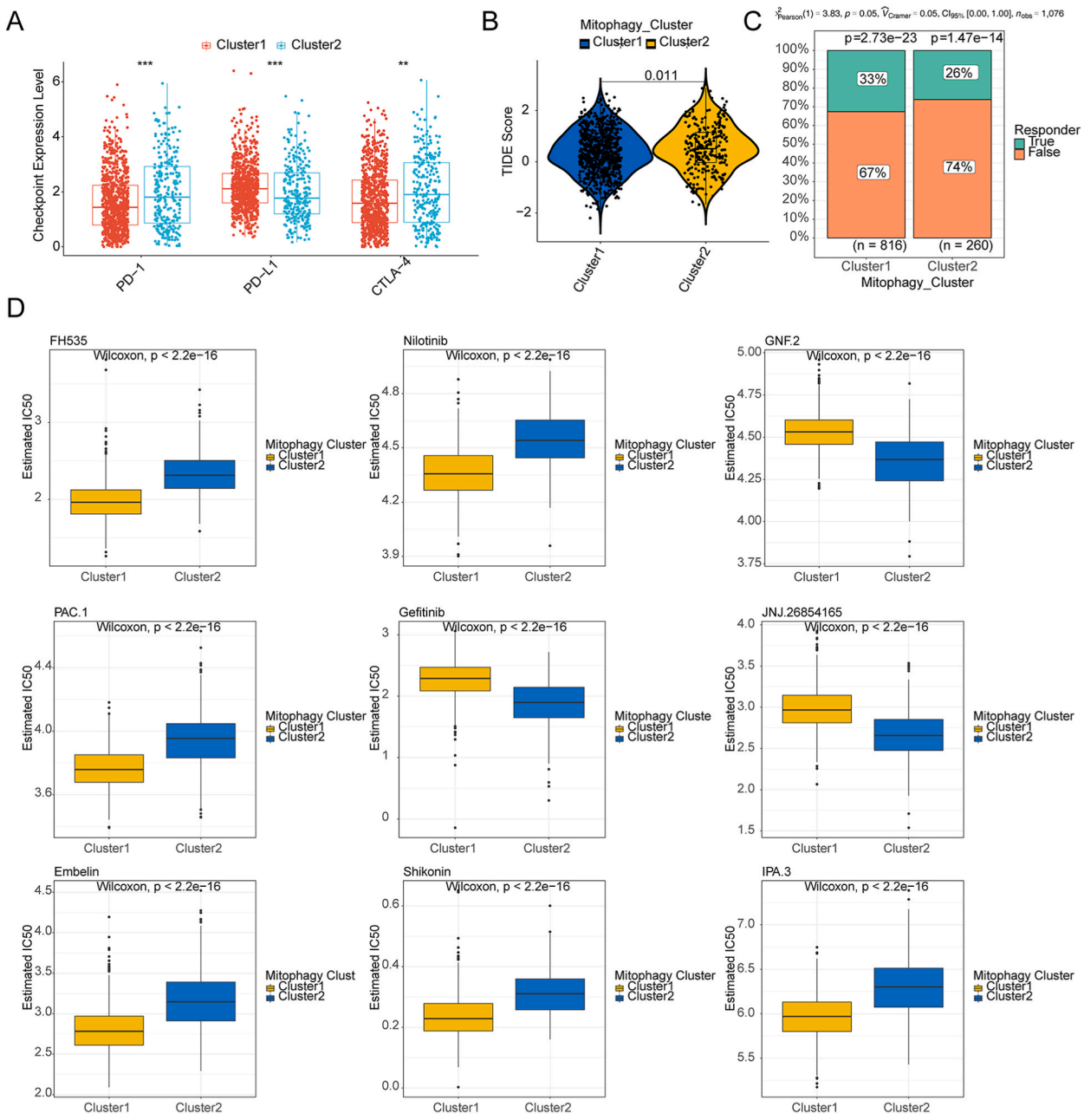

Fig. 7. The relationship between mitophagy-related subtypes and immunotherapy and drug sensitivity. (**A**)The expression of three immune checkpoints between two subtypes. Differences in (**B**) the TIDE score and (**C**) immunotherapy response of two subtypes. (**D**) The top 9 drugs with the highest sensitivity differences between two subtypes.

and PC2 (Mitophagy score) calculated in METABRIC-PCA (Fig. S2B), and obtained cluster 1 and cluster 2 corresponding to METABRIC data set. Our findings were replicated in the METABRIC dataset ($P < 0.0001$) (Fig. S2C). The results of Wilcoxon test indicated that the levels of three immune markers (APM: $P < 0.0001$, TILs: $P < 0.05$, TIS: $P < 0.0001$) and three immune checkpoints (PD-1: $P < 0.0001$, PD-L1: $P < 0.001$, CTLA-4: $P < 0.0001$) in cluster2 were higher than that in cluster1 except for CYT ($P > 0.05$) (Figs. S2D–E).

4. Discussion

Breast cancer is a highly heterogeneous tumor. The molecular type of breast cancer is increasingly completed and constantly updated, and research as well as therapy for breast cancer thus awarded significant progression. Whereas, the problem of advanced breast cancer and therapeutic resistance still needs to be resolved. A growing body of evidence has suggested that mitophagy has a great relationship with tumor, including breast cancer [2,7].

We divided 1076 samples in TCGA-BRCA into two subtypes based on the expression of 29 mitophagy-related genes. Notably, cluster1 had a high expression of mitophagy-related genes with worse survival, which implied the close linkage between mitophagy and prognosis of BRCA patients. Interestingly, the proportion of triple-negative breast cancer and metastatic breast cancer in cluster2 was higher compared with cluster1. Given the dual role of mitophagy in cancer and the mechanism of mitophagy in BRCA was unclear, we further explored the cause of phenotypic difference between two subtypes, and analyses of biological characteristics, genomic background and immune features were done.

We first analyzed the biological features of subtypes. In the 42 pathways with significant differences, cluster2 was significantly correlated with TNFA signaling via NFkb, IL6-JAK-STAT3, p53 pathway and KRAS signaling pathways which play an important role in promoting tumor growth, invasion and metastasis [24–26]. Otherwise, cluster2 was characterized by significant activation of hypoxia, oxidative phosphorylation, glycolysis and reactive oxygen species pathway, all of which are crucial signaling pathways that regulate metabolism and tumor development [27–29]. Based on the above result, we speculated that excess ROS produced in cluster2 may be associated with lower expression of mitophagy-related genes. Furthermore, immune-related pathways (notch signaling, interferon alpha response, interferon gamma response and inflammatory response) were enriched in cluster2. Interferon, as prototypic immunotherapeutics, have resulted in improved outcomes for patients with malignancies of heterogeneous histologies [30]. However, in breast cancer, notch signaling played a stimulative role in *trans*-endothelial tumor cell migration, metastasis and chemotherapy resistance [31–33]. Seven pathways were enriched in cluster1, including mitotic spindle, TGF beta signaling, and hedgehog signaling pathway, which were linked to proliferation and tumor development [34,35]. Interestingly, in the early cancer cells, the TGF beta signaling pathway has functions of cell-cycle arrest and apoptosis as a tumor-suppressor, but it can promote tumorigenesis in the late stage, including metastasis and chemoresistance [35]. In addition, cluster1 was also significantly correlated with cancer-related malignant signaling pathways, such as HIPPO, NOTH, PI3K, TGF-b, RTK/RAS and TP53. These pathways are crucial pathways that can regulate cancer proliferation, invasion, metastasis and immunologic escape, and abnormal activation of them promotes tumor malignancy and contribute to poor prognosis [36–38].

ESTIMATE was used to estimate the proportion of stromal cells and immune cells in malignant tissue to assess tumour purity which was the proportion of tumor cells in tumor tissue. Non-tumor cells in tumor played an important role in tumor growth, progression, or drug resistance, such as stromal or interstitial cells that promote tumor growth and affect tumor response [39], while immune cells such as cytotoxic T lymphocytes (CTLs) may inhibit tumor growth [40]. In TNBC, high stromal content was related to a relatively poor prognosis [41,42]. Cluster2 had higher tumor immunogenicity and lower tumor purity than cluster1, which means cluster1 with a stronger invasion ability, may be related to its poor prognosis. Differences in immune cell composition of the microenvironment may be the potential immune biomarkers and supplied reference for tumor development and response to immunotherapy. TIDE was used to predict the response to immune checkpoint inhibitors and assess sensitivity of immunotherapy. In other words, it can assess the potential for immune escape based on the gene expression profile of cancer samples [43,44]. The result of TIDE indicated that cluster2 had a higher potential of immune escape and lower response to immunotherapy, and the expression of PD-1, PD-L1 and CTLA-4 showed that cluster2 may have a lower response to inhibitors of PD-L1, which provided a new reference for BRCA immunotherapy. Otherwise, the analysis of chemotherapy provided references for treatments of mitophagy-related subtypes and difficult problems of resistance in clinical.

In summary, our research first proposed a new classification based on the mitophagy of breast cancer and further explored the clinical and molecular characteristics of subtypes. The results of analyses simultaneously proved the possibility and validity of this typing. Fewer studies explained the relationship between mitophagy and breast cancer, we provided data support and direction for deeper research. In addition, the mitochondrial autophagy-related typing in this study is expected to assess the stage and prognosis of BRCA and apply anti-autophagic therapy as a possible treatment for BRCA. Although pathway analysis and functional enrichment analysis were used to initially explain the biological significance of clustering results, the results could not explain the specific biological differences between samples, and further experimental validation and clinical data support were needed.

Availability of data

The datasets generated during the current study were available in The Cancer Genome Atlas (TCGA, xenabrowser.net) and The Reactome database (reactome.org/). METABRIC dataset containing BRCA samples was downloaded from cBioPortal as a external validation datasets.

CRediT authorship contribution statement

Yaqing Zhou: Data curation, Formal analysis, Writing – original draft. **Xing Wei:** Data curation, Formal analysis. **Weimiao Li:** Data curation, Formal analysis. **Shuqun Zhang:** Methodology, Supervision. **Yonglin Zhao:** Conceptualization, Data curation, Formal analysis, Writing – review & editing.

Declaration of competing interest

The authors declare that they have no known competing financial interests or personal relationships that could have appeared to influence the work reported in this paper.

Appendix A. Supplementary data

Supplementary data to this article can be found online at https://doi.org/10.1016/j.heliyon.2023.e23267.

References

[1] H. Sung, J. Ferlay, R.L. Siegel, M. Laversanne, I. Soerjomataram, A. Jemal, F. Bray, Global cancer statistics 2020: GLOBOCAN estimates of incidence and mortality worldwide for 36 cancers in 185 countries, CA: Cancer J. Clin. 71 (2021), https://doi.org/10.3322/caac.21660.

[2] A.G. Waks, E. P Winer, Breast cancer treatment: a review, JAMA 321 (2019) 288–300. https://doi:10.1001/jama.2018.19323.

[3] M.F. Mustafa, S.M. Saliluddin, S. Fakurazi, N.M.S. Tizen Laim, S.H. Md Pauzi, N.H. Nik Yahya, N. S Raja Gopal, M.A. Abdullah, S. Maniam, Expression of autophagy and mitophagy markers in breast cancer tissues, Front. Oncol. 11 (2021), 612009, https://doi.org/10.3389/fonc.2021.612009.

[4] C.M. Perou, T. Sørlie, M.B. Eisen, M. van de Rijn, S.S. Jeffrey, C.A. Rees, J.R. Pollack, D.T. Ross, H. Johnsen, L.A. Akslen, O. Fluge, A. Pergamenschikov, C. Williams, S.X. Zhu, P.E. Lønning, A.L. Børresen-Dale, P.O. Brown, D. Botstein, Molecular portraits of human breast tumours, Nature 406 (2000) 747–752. https://doi:10.1038/35021093.

[5] E.S. McDonald, A.S. Clark, J. Tchou, P. Zhang, G.M. Freedman, Clinical diagnosis and management of breast cancer, J. Nucl. Med. 57 (Suppl 1) (2016) 9S–16S. https://doi:10.2967/jnumed.115.157834.

[6] J.E. Lang, J.S. Wecsler, M.F. Press, D. Tripathy, Molecular markers for breast cancer diagnosis, prognosis and targeted therapy, J. Surg. Oncol. 111 (2015) 81–90, https://doi.org/10.1002/jso.23732.

[7] N. Mizushima, M. Komatsu, Autophagy: renovation of cells and tissues, Cell 147 (2011) 728–741. https://doi:10.1016/j.cell.2011.10.026.

[8] I. Kim, S. Rodriguez-Enriquez, J.J. Lemasters, Selective degradation of mitochondria by mitophagy, Arch. Biochem. Biophys. 462 (2007) 245–253. https://doi:10.1016/j.abb.2007.03.034.

[9] K. Palikaras, E. Lionaki, N. Tavernarakis, Mechanisms of mitophagy in cellular homeostasis, physiology and pathology, Nat. Cell Biol. 20 (2018) 1013–1022. https://doi:10.1038/s41556-018-0176-2.

[10] P.P. Naik, A. Birbrair, S.K. Bhutia, Mitophagy-driven metabolic switch reprogr-ams stem cell fate, Cell. Mol. Life Sci. 76 (2019) 27–43. https://doi:10.1007/s00018-018-2922-9.

[11] Y. Zhao, Y. Zhang, C. Dai, K. Hong, Y. Guo, A signature constructed with mitophagy-related genes to predict the prognosis and therapy response for breast cancer, Aging (Albany NY) 14 (15) (2022) 6169–6186. https://doi:10.18632/aging.204209.

[12] Y. Wang, Z. Wang, J. Sun, Y. Qian, Identification of HCC subtypes with different prognosis and metabolic patterns based on mitophagy, Front. Cell Dev. Biol. 9 (2021), 799507. https://doi:10.3389/fcell.2021.799507.

[13] M.D. Wilkerson, D.N. Hayes, ConsensusClusterPlus: a class discovery tool with confidence assessments and item tracking, Bioinformatics 26 (2010) 1572–1573. https://doi:10.1093/bioinformatics/btq170.

[14] Z. Gu, R. Eils, M.G. Schlesner, Complex heatmaps reveal patterns and correlations in multidimensional genomic data, Bioinformatics (Oxford, England) (2016) 32, https://doi.org/10.1093/bioinformatics/btw313.

[15] A. Mayakonda, D.C. Lin, Y. Assenov, C. Plass, H.P. Koeffler, Maftools: efficient and comprehensive analysis of somatic variants in cancer, Genome Res. 28 (2018) 1747–1756, https://doi.org/10.1101/gr.239244.118.

[16] C.H. Mermel, S.E. Schumacher, B. Hill, M.L. Meyerson, R. Beroukhim, G. Getz, GISTIC2.0 facilitates sensitive and confident localization of the targets of focal somatic copy-number alteration in human cancers, Genome Biol. 12 (2011) R41. https://doi:10.1186/gb-2011-12-4-r41.

[17] Y. Xu, W. Liao, Q. Luo, D. Yang, M. Pan, Histone acetylation regulator-mediated acetylation patterns define tumor malignant pathways and tumor microenvironment in hepatocellular carcinoma, Front. Immunol. 13 (2022), 761046. https://doi:10.3389/fimmu.2022.761046.

[18] V. Thorsson, D.L. Gibbs, S.D. Brown, D. Wolf, D.S. Bortone, T.H. Ou Yang, E. Porta Pardo, G.F. Gao, The immune landscape of cancer, Immunity 48 (2018) 812–830. https://doi:10.1016/j.immuni.2018.03.023.

[19] G. Bindea, B. Mlecnik, M. Tosolini, A. Kirilovsky, M. Waldner, A.C. Obenauf, H. Angell, Spatiotemporal dynamics of intratumoral immune cells reveal the immune landscape in human cancer, Immunity 39 (2013) 782–795. https://doi:10.1016/j.immuni.2013.10.003.

[20] K. Yoshihara, M. Shahmoradgoli, E. Martínez, R. Vegesna, H. Kim, W. Torres-Garcia, V. Treviño, Inferring tumour purity and stromal and immune cell admixture from expression data, Nat. Commun. 4 (2013) 2612. https://doi:10.1038/ncomms3612.

[21] A.M. Newman, C.L. Liu, M.R. Green, A.J. Gentles, W. Feng, Y. Xu, C.D. Hoang, M. Diehn, A.A. Alizadeh, Robust enumeration of cell subsets from tissue expression profiles, Nat. Methods 12 (2015) 453–457. https://doi:10.1038/nmeth.3337.

[22] P. Jiang, S. Gu, D. Pan, J. Fu, A. Sahu, X. Hu, Z. Li, N. Traugh, X. Bu, B. Li, J. Liu, G.J. Freeman, M.A. Brown, K.W. Wucherpfennig, X.S. Liu, Signatures of T cell dysfunction and exclusion predict cancer immunotherapy response, Nat. Med. 24 (2018) 1550–1558. https://doi:10.1038/s41591-018-0136-1.

[23] P. Geeleher, N. Cox, R.S. Huang, pRRophetic: an R package for prediction of clinical chemotherapeutic response from tumor gene expression levels, PLoS One 9 (2014), e107468. https://doi:10.1371/journal.pone.0107468.

[24] J. De, O. Ra, G. Jr, Targeting the IL-6/JAK/STAT3 signalling axis in cancer, Nat. Rev. Clin. Oncol. 15 (2018), https://doi.org/10.1038/nrclinonc.2018.8.

[25] Y. Wu, B.P. Zhou, TNF-alpha/NF-kappaB/Snail pathway in cancer cell migration and invasion, Br. J. Cancer 102 (2010) 639–644. https://doi:10.1038/sj.bjc.6605530.

[26] H.J. Kim, H.N. Lee, M.S. Jeong, S.B. Jang, Oncogenic KRAS: signaling and drug resistance, Cancers 13 (2021) 5599, https://doi.org/10.3390/cancers13225599.

[27] A.P. Nayak, A. Kapur, L. Barroilhet, M.S. Patankar, Oxidative Phosphorylation: a target for novel therapeutic strategies against ovarian cancer, Cancers 10 (2018) 337. https://doi:10.3390/cancers10090337.

[28] J. Chen, C.E. Mathews, Use of chemical probes to detect mitochondrial ROS by flow cytometry and spectrofluorometry, Methods Enzymol. (2014) 542, https://doi.org/10.1016/B978-0-12-416618-9.00012-1.

[29] L. Schito, G.L. Semenza, Hypoxia-inducible factors: master regulators of cancer progression, Trends Cancer 2 (2016), https://doi.org/10.1016/j.trecan.2016.10.016.

[30] E.C. Borden, Interferonsαandβin cancer: therapeutic opportunities from new insights, Nat. Rev. Drug Discov. 18 (2019) 219–234. https://doi:10.1038/s41573-018-0011-2.

[31] J. Pignatelli, J.J. Bravo-Cordero, M. Roh-Johnson, S.J. Gandhi, Y. Wang, X. Chen, R.J. Eddy, A. Xue, R.H. Singer, L. Hodgson, M.H. Oktay, J.S. Condeelis, Macrophage-dependent tumor cell transendothelial migration is mediated by Notch1/MenaINV-initiated invadopodium formation, Sci. Rep. 6 (2016), 37874. https://doi:10.1038/srep37874.

[32] N. Sethi, X. Dai, C.G. Winter, Y. Kang, Tumor-derived JAGGED1 promotes osteolytic bone metastasis of breast cancer by engaging notch signaling in bone cells, Cancer Cell 19 (2011) 192–205. https://doi:10.1016/j.ccr.2010.12.022.

[33] M.C. Boelens, T.J. Wu, B.Y. Nabet, B. Xu, Y. Qiu, T. Yoon, D.J. Azzam, C. Twyman-Saint Victor, B.Z. Wiemann, H. Ishwaran, P.J. Ter Brugge, J. Jo-nkers, J. Slingerland, A.J. Minn, Exosome transfer from stromal to breast cancer cells regulates therapy resistance pathways, Cell 159 (2014) 499–513. https://doi:10.1016/j.cell.2014.09.051.
[34] A.M. Skoda, D. Simovic, V. Karin, V. Kardum, S. Vranic, L. Serman, The role of the Hedgehog signaling pathway in cancer: a comprehensive review, Bosn. J. Basic Med. Sci. 18 (2018) 8–20. https://doi:10.17305/bjbms.2018.2756.
[35] S. Colak, P. Ten Dijke, Targeting TGF-βsignaling in cancer, Trends Cancer 3 (2017) 56–71. https://doi:10.1016/j.trecan.2016.11.008.
[36] S. Zhang, D. Zhou, Role of the transcriptional coactivators YAP/TAZ in liver cancer, Curr. Opin. Cell Biol. 61 (2019) 64–71. https://doi:10.1016/j.ceb.2019.07.006.
[37] C. Zhu, Y.J. Ho, M.A. Salomao, D.H. Dapito, A. Bartolome, R.F. Schwabe, J.S. Lee, S.W. Lowe, U.B. Pajvani, Notch activity characterizes a common hepatocellular carcinoma subtype with unique molecular and clinicopathologic features, J. Hepatol. 74 (2021) 613–626. https://doi:10.1016/j.jhep.2020.09.032.
[38] X. Wang, J. Wang, Y.M. Tsui, C. Shi, Y. Wang, X. Zhang, Q. Yan, M. Chen, C. Jiang, Y.F. Yuan, C.M. Wong, M. Liu, Z.Y. Feng, H. Chen, I.O.L. N-g, L. Jiang, X. Y. Guan, RALYL increases hepatocellular carcinoma stemness by sustaining the mRNA stability of TGF-β2, Nat. Commun. 12 (2021) 1518. https://doi:10.1038/s41467-021-21828-7.
[39] M.R. Junttila, F.J. de Sauvage, Influence of tumour micro-environment heterogeneity on therapeutic response, Nature 501 (2013) 346–354. https://doi:10.1038/nature12626.
[40] F. Pagès, J. Galon, M.C. Dieu-Nosjean, E. Tartour, C. Sautès-Fridman, W.H. Fridman, Immune infiltration in human tumors: a prognostic factor that should not be ignored, Oncogene 29 (2010) 1093–1102. https://doi:10.1038/onc.2009.416.
[41] A.M. Moorman, R. Vink, H.J. Heijmans, J. van der Palen, E.A. Kouwenhoven, The prognostic value of tumour-stroma ratio in triple-negative breast cancer, Eur. J. Surg. Oncol. 38 (2012) 307–313, https://doi.org/10.1016/j.ejso.2012.01.002.
[42] C.J.H. Kramer, K.M.H. Vangangelt, G.W. van Pelt, T.J.A. Dekker, R.A.E.M. Tollenaar, W.E. Mesker, The prognostic value of tumour-stroma ratio in primary breast cancer with special attention to triple-negative tumours: a review, Breast Cancer Res. Treat. 173 (2019) 55–64. https://doi:10.1007/s10549-018-4987-4.
[43] J. Fu, K. Li, W. Zhang, C. Wan, J. Zhang, P. Jiang, X.S. Liu, Large-scale public data reuse to model immunotherapy response and resistance, Genome Med. 12 (2020) 21. https://doi:10.1186/s13073-020-0721-z.
[44] P. Jiang, S. Gu, D. Pan, J. Fu, A. Sahu, X. Hu, Z. Li, N. Traugh, X. Bu, B. Li, J. Liu, G.J. Freeman, M.A. Brown, K.W. Wucherpfennig, X.S. Liu, Signatures of T cell dysfunction and exclusion predict cancer immunotherapy response, Nat. Med. 24 (2018) 1550–1558. https://doi:10.1038/s41591-018-0136-1.